Supplemental Data

Methods

Immunofluorescence confocal microscopy

Immunofluorescence confocal microscopy was used to assess the influence c.[2365A>G;2385T>C] genotype on intracellular localization and pseudo-Weibel-Palade body formation. Briefly, HEK293 cells were transiently transfected with equimolar concentrations of wild-type or c.[2365A>G;2385T>C] VWF expression plasmid using Lipofectamine™ (Thermo Fisher Scientific, Carlsbad, CA, USA) according to manufacturer's protocols. Post-transfection (24 h) cells were fixed using BD Cytofix/Cytoperm™ (BD Biosciences, Mississauga, ON, Canada), permeabilized using 0.1% Triton X-100 and blocked using Protein Block (Dako, Glostrup, Denmark). Cells were stained with an anti-VWF antibody (A0082; Dako), DAPI and Alexa Fluor® 647 phalloidin (Thermo Fisher). Slides were imaged using a Leica SP8 laser scanning confocal microscope using a 63X oil immersion objective (Leica Microsystems Inc., Concord, ON, Canada).

RNA splicing assays

Two different *in vitro* minigene splicing assays were utilized to investigate RNA splicing. The pET01 Exontrap plasmid (MoBiTec GmbH, Goettingen, Germany) was used to investigate any influence on acceptor / donor splice sites. Wild-type (WT) VWF DNA for exon 18 and ~300 bp flanking intronic sequence was inserted into pET01 via restriction enzyme-mediated cloning. Site-directed mutagenesis was used to generate pET01 plasmids encoding c.2365A>G, c.2385T>C and c.[2365A>G;2385T>C]. An exonic splice enhancer (ESE)-dependent splicing assay[1] utilizing the pcDNA-Dup (SF2-ASF3x) plasmid (kindly provided by Dr. Pascaline Gaildrat, University of Rouen, France) was used to investigate any influence on ESE motifs. Oligonucleotides containing SNV alleles of interest (reference and non-reference) and 15 bp flanking DNA sequence (details available on request) were inserted within the middle exon of pcDNA-Dup via restriction enzyme-mediated cloning. Plasmids containing a functional SF2/ASF ESE or a region of intronic DNA with no predicted ESE motif were used as positive and negative controls respectively. Generated pET01 or pcDNA-Dup plasmids were transfected into HEK293T cells, mRNA was isolated and reverse transcribed to cDNA. Agarose gel electrophoresis was used to separate specific cDNA products.

VWF:FVIIIB analysis

The ability of recombinant VWF secreted by HEK293T cells to bind FVIII was evaluated using an ELISA as previously described, but with minor modifications.[2,3] Briefly, 10 mU/well of recombinant VWF concentrated by centrifugation (Centricon Plus-70 Centrifugal Filter, 100 kDa pore size; Millipore (Canada) Ltd., Etobicoke, ON) was captured on a 96 well plate coated with an anti-VWF antibody (A0082; Dako, Glostrup, Denmark) and 0.06-2.0 IU/mL recombinant FVIII (ADVATE, Baxter, Deerfield, IL, USA) and incubated for 1 h at 37°C in 10 mM calcium-containing buffer. Bound FVIII was measured with a HRP-conjugated anti-human FVIII antibody (F8C-EIA-D; Affinity Biologicals Inc., Ancaster, ON, Canada). Binding plots were fitted with a one-site binding model (hyperbola) and apparent dissociation rate constant values (Kd^{app}) were obtained. The best-fit Kd^{app} values of VWF SNV were statistically compared to that of WT VWF using an *F*-test.

In order to evaluate precise binding kinetics, WT and p.[T789A;Y795=] VWF were purified with immunoaffinity chromatography using monoclonal antibody CLB-RAg20 and a CNBr sepharose 4B column (performed by Jesse Lai with support from Dr. Jan Voorberg, Department of Plasma Proteins, Sanquin Research, Amsterdam, The Netherlands).[4] A surface plasmon resonance (SPR) assay (using a Biacore 3000; GE Healthcare Bio-Sciences, Pittsburgh, PA, USA) was then performed on purified VWF as previously described.[5] Briefly, purified VWF was covalently immobilized on a C1 sensor chip at a coupling density of 2.0 ng/mm^3 and FVIII (0.313-10 nM; ADVATE) was injected at a rate of 10 µl/min for 4 min (association phase) and flown-out with buffer for 4 min (dissociation phase). The chip surface was regenerated with 4 M $MgCl_2$, 1 M NaCl solution. Binding to the surface of the control uncoated flow cell was subtracted from binding to VWF-coated flow cells. Measurements were performed at 37°C. BIAevaluation v2.1 (GE Healthcare) was used to estimate kinetic rate constants and to perform nonlinear regression analysis to determine the rate constants for association (ka) and dissociation (kd). Dissociation constants (KD) were calculated as kd/ka.

Table S1. Predicted *in silico* effect of SNV on protein and RNA

Prediction tool		c.2365A>G	c.2385T>C
Protein predictions	Mutation Taster[6]	Polymorphism	NA
	PolyPhen-2[7]	Benign	NA
	PON-P2[8]	Neutral	NA
	PROVEAN[9]	Neutral	NA
	SIFT[10]	Tolerated	NA
RNA predictions	CentroidFold[11]	Alters secondary structure	Alters secondary structure
	miRBase[12,13]	No effect	No effect
Splicing predictions	ESEfinder*[,14]	No effect	Creates SRp55 motif, weakens SC35 motif
	HSF[15]	Creates ESS motif, cryptic donor activation	No effect
	NetGene2†[,16]	Cryptic donor activation	No effect
	Neural Network†[,17]	No effect	No effect
	RESCUE-ESE*[,18]	No effect	Creates ESE motif
	SplicePort†[,19]	Cryptic donor activation, weakens existing donor	Cryptic acceptor activation, cryptic donor activation, weakens existing donor

ESE, exonic splice enhancer; ESS, exonic splice silencer; NA, not applicable. *ESE / ESS predictions only; †acceptor / donor predictions only.

Table S2. Influence of SNV on VWF:FVIIIB

Expressed VWF	VWF:FVIIIB* Kd^{app} (nM)	VWF:FVIIIB† ka x 10^6	kd x 10^{-3}	KD (nM)
Wild-type	0.10 ± 0.01	2.98 ± 0.015	1.63 ± 0.019	0.545
p.T789A	0.12 ± 0.01	nd	nd	nd
p.Y795=	0.11 ± 0.01	nd	nd	nd
p.[T789A;Y795=]	0.12 ± 0.01	2.98 ± 0.022	2.32 ± 0.030	0.777
p.T789P	No binding	nd	nd	nd

ka, association rate constant; kd, dissociation rate constant; KD, equilibrium dissociation constant; Kd^{app}, apparent dissociation rate constant; nd, not determined. *VWF:FVIIIB determined by ELISA; †VWF:FVIIIB determined by SPR.

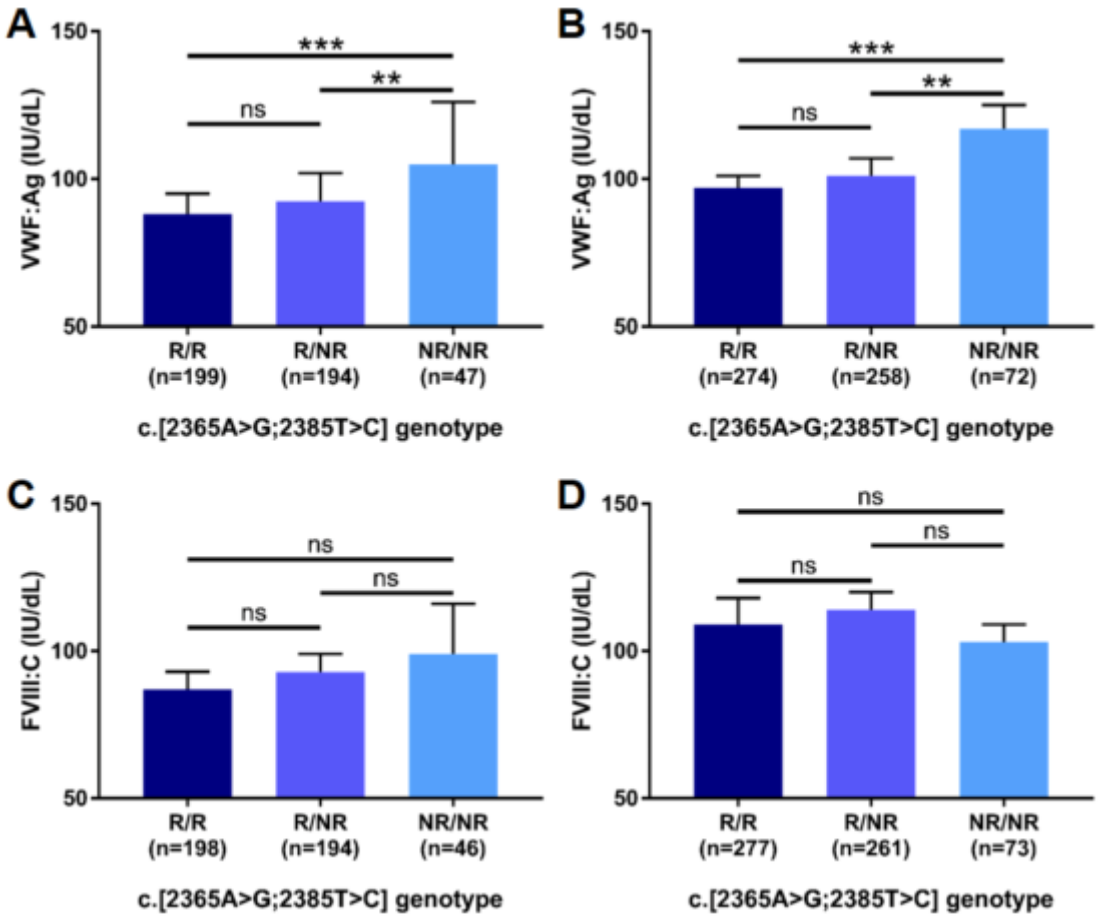

Figure S1. Association between SNV c.[2365A>G;2385T>C] genotype and median VWF:Ag and FVIII:C levels accounting for ABO blood group. (A) VWF:Ag in O blood group individuals. (B) VWF:Ag in non-O blood group individuals. (C) FVIII:C in O blood group individuals. (D) FVIII:C in non-O blood group individuals. NR, non-reference allele; R, reference allele. Genotypes compared using a Mann-Whitney test (**, $p<0.01$; ***, $p<0.001$; ns, not significant). Bars indicate 95% confidence interval.

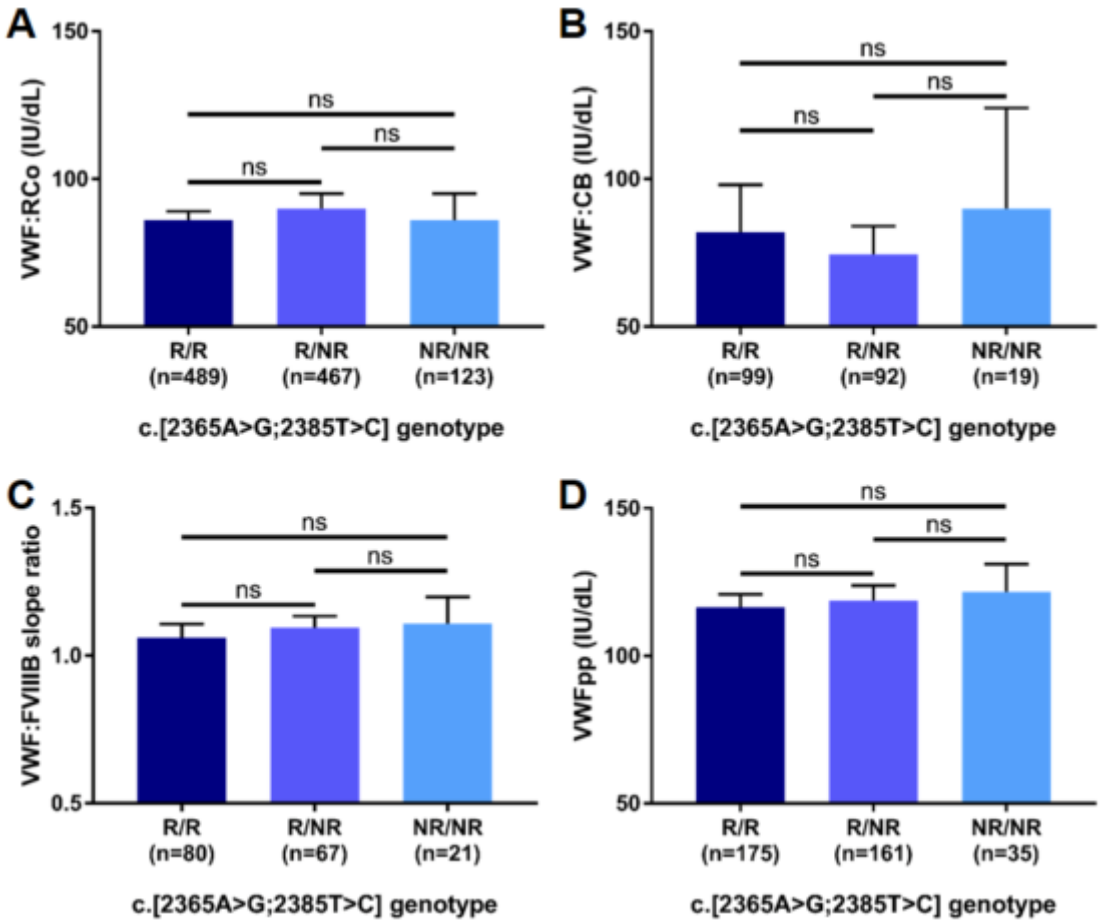

Figure S2. Association between SNV c.[2365A>G;2385T>C] genotype and VWF activity / propeptide levels in healthy controls. (A) Median VWF:RCo levels. (B) Median VWF:CB levels. (C) Median VWF:FVIIIB slope ratio. (D) Median VWFpp levels. NR, non-reference allele; R, reference allele. Genotypes compared using a Mann-Whitney test (ns, not significant). Bars indicate 95% confidence interval.

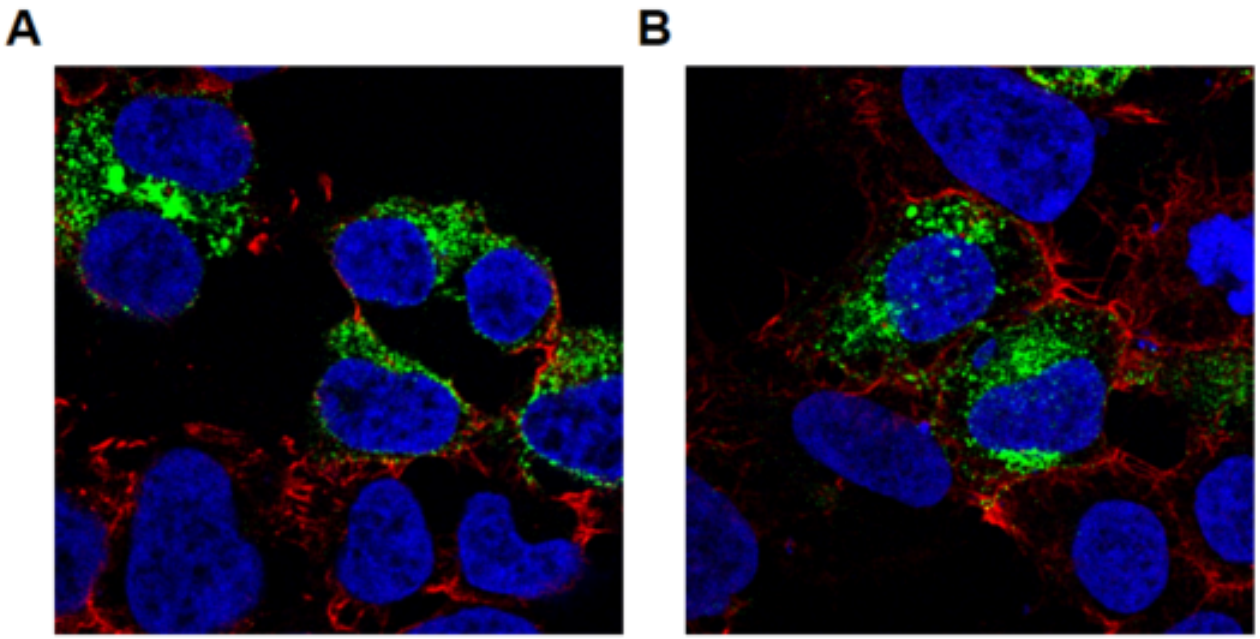

Figure S3. Intracellular localization and pseudo-Weibel-Palade body formation for wild-type (A) and c.[2365A>G;2385T>C] (B) VWF. Blue, nucleus; green, VWF; red, F-actin.

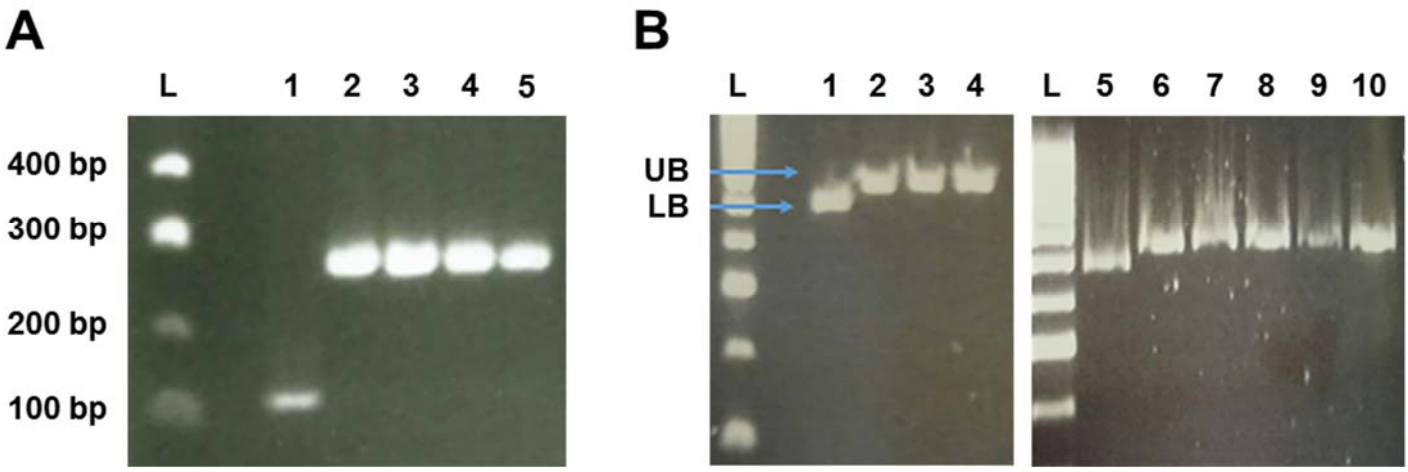

Figure S4. *In vitro* analysis of SNV effect on splicing. (A) Influence on acceptor / donor splice sites (lane 1: negative control; lane 2: WT; lane 3: c.2385T>C; lane 4: c.2365A>G; lane 5: c.[2365A>G;2385T>C]). (B) Influence on exonic splice enhancer motifs (lanes 1 and 5: negative control; lanes 2 and 6: positive control; lanes 3, 7 and 9: WT; lane 4: c.2385T>C; lane 8: c.2365A>G; lane 10: c.[2365A>G;2385T>C]). L, HyperLadder 100bp; LB, lower band (i.e. 2 exons); UB, upper band (i.e. 3 exons).

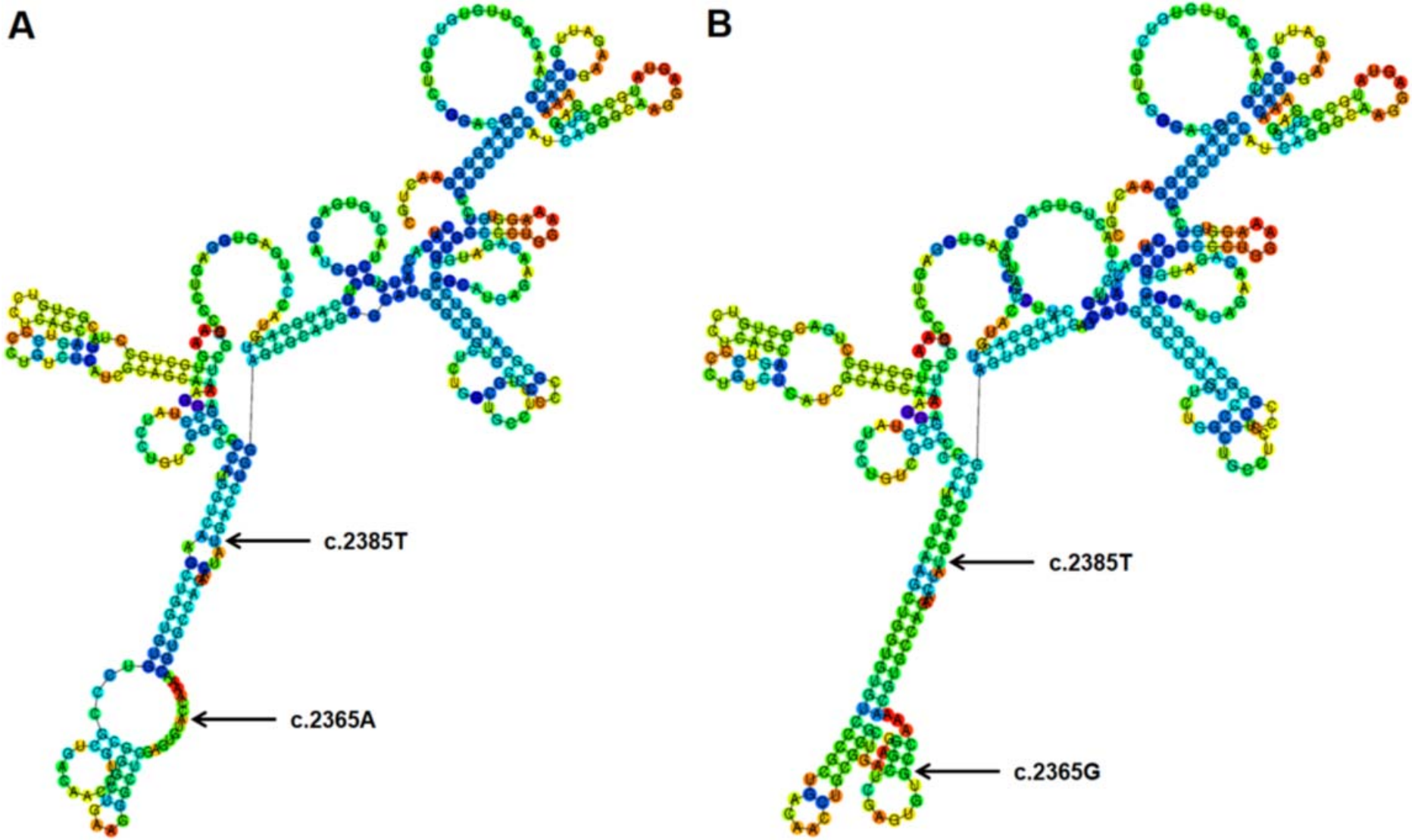
A
c.2385T
c.2365A
B
c.2385T
c.2365G

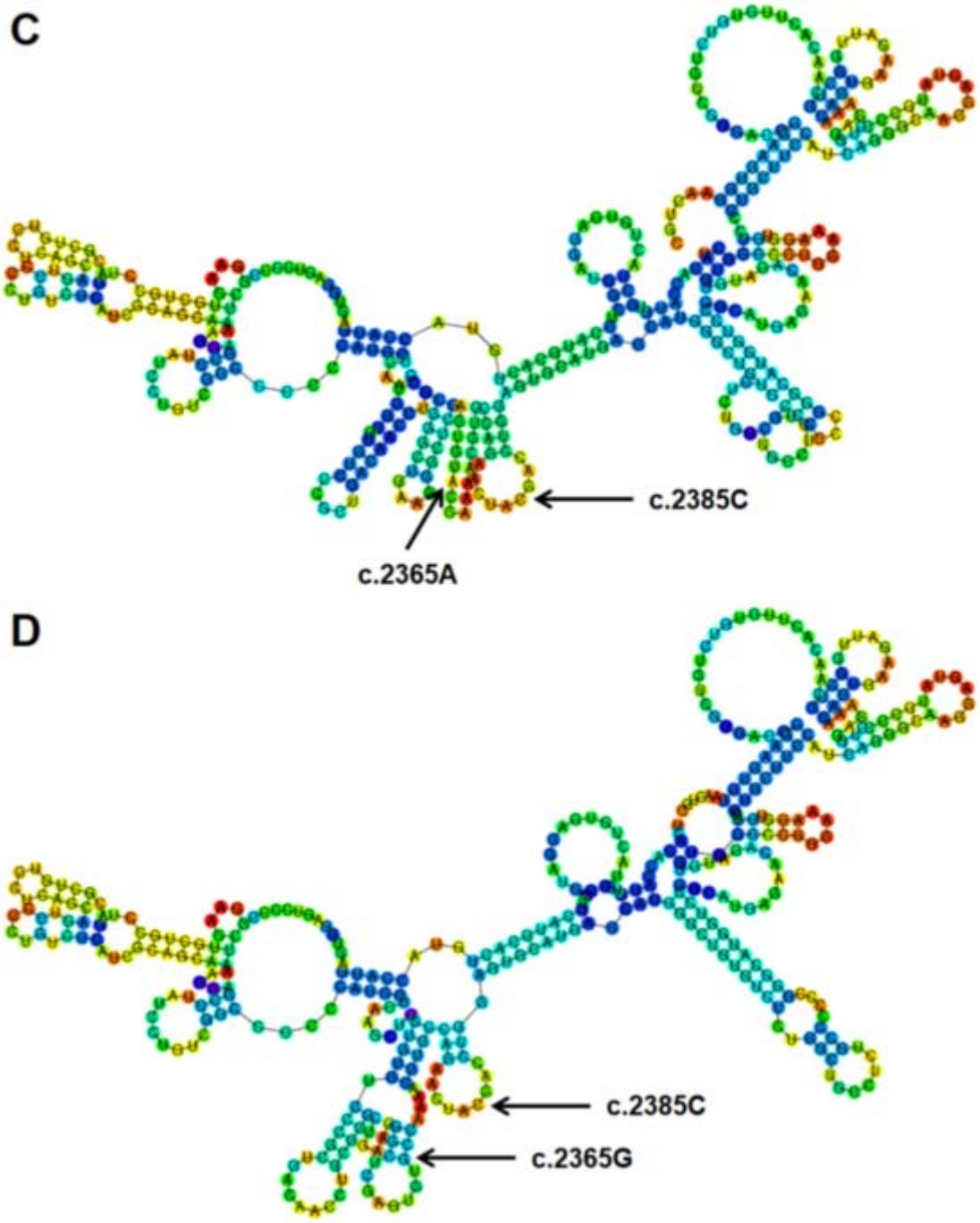

Figure S5. RNA secondary structure predictions. (A) Wild-type. (B) c.2365A>G. (C) c.2385T>C. (D) c.[2365A>G;2385T>C]. Data generated with CentroidFold[11] using default settings.

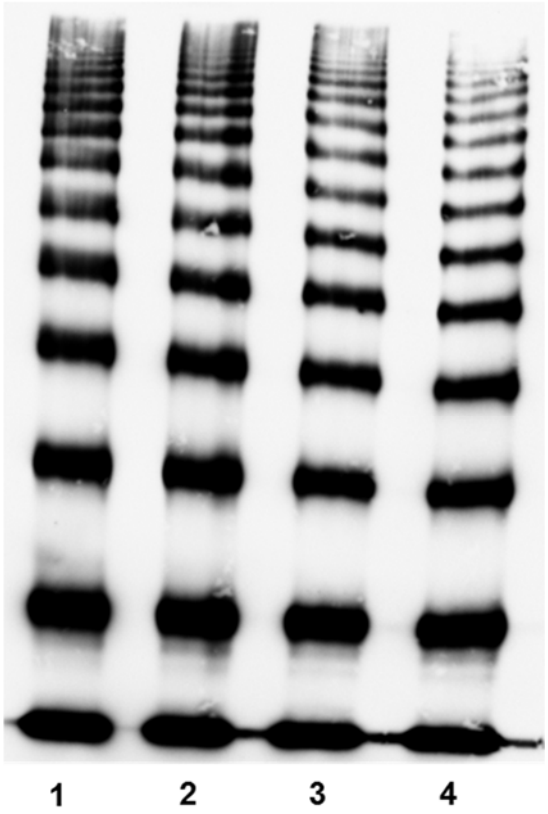

Figure S6. Multimers profiles of expressed recombinant VWF. Multimer analysis of secreted VWF was performed via electrophoresis on a 1.6% (w/v) SDS-agarose gel (lane 1: wild-type; lane 2: c.2365A>G; lane 3: c.2385T>C; lane 4: c.[2365A>G;2385T>C]).

References

1. Tournier I, Vezain M, Martins A, et al. A large fraction of unclassified variants of the mismatch repair genes *MLH1* and *MSH2* is associated with splicing defects. *Hum Mutat*. 2008;29(12):1412-1424.
2. Taylor SL, Bromidge E, Savidge GF, Alhaq A. Evaluation of an automated screening assay for von Willebrand disease type 2N. *Clin Lab Haematol*. 2002;24(6):369-375.
3. Zhukov O, Popov J, Ramos R, et al. Measurement of von Willebrand factor-FVIII binding activity in patients with suspected von Willebrand disease type 2N: application of an ELISA-based assay in a reference laboratory. *Haemophilia*. 2009;15(3):788-796.
4. van den Biggelaar M, Bierings R, Storm G, Voorberg J, Mertens K. Requirements for cellular co-trafficking of factor VIII and von Willebrand factor to Weibel–Palade bodies. *J Thromb Haemost*. 2007;5(11):2235-2242.
5. Dimitrov JD, Christophe OD, Kang J, et al. Thermodynamic analysis of the interaction of factor VIII with von Willebrand factor. *Biochemistry*. 2012;51(20):4108-4116.
6. Schwarz JM, Cooper DN, Schuelke M, Seelow D. MutationTaster2: mutation prediction for the deep-sequencing age. *Nat Methods*. 2014;11(4):361-362.
7. Adzhubei IA, Schmidt S, Peshkin L, et al. A method and server for predicting damaging missense mutations. *Nat Methods*. 2010;7(4):248-249.
8. Niroula A, Urolagin S, Vihinen M. PON-P2: prediction method for fast and reliable identification of harmful variants. *PLoS One*. 2015;10(2):e0117380.
9. Choi Y, Chan AP. PROVEAN web server: a tool to predict the functional effect of amino acid substitutions and indels. *Bioinformatics*. 2015;31(16):2745-2747.
10. Kumar P, Henikoff S, Ng PC. Predicting the effects of coding non-synonymous variants on protein function using the SIFT algorithm. *Nat Protoc*. 2009;4(7):1073-1081.
11. Hamada M, Ono Y, Kiryu H, et al. Rtools: a web server for various secondary structural analyses on single RNA sequences. *Nucleic Acids Res*. 2016;44(Web Server issue):W302-307.
12. Griffiths-Jones S, Saini HK, van Dongen S, Enright AJ. miRBase: tools for microRNA genomics. *Nucleic Acids Res*. 2008;36(Database issue):D154-158.

13. Kozomara A, Griffiths-Jones S. miRBase: integrating microRNA annotation and deep-sequencing data. *Nucleic Acids Res*. 2011;39(Database issue):D152-157.
14. Cartegni L, Wang J, Zhu Z, Zhang MQ, Krainer AR. ESEfinder: a web resource to identify exonic splicing enhancers. *Nucleic Acids Res*. 2003;31(13):3568-3571.
15. Desmet F-O, Hamroun D, Lalande M, Collod-Béroud G, Claustres M, Béroud C. Human Splicing Finder: an online bioinformatics tool to predict splicing signals. *Nucleic Acids Res*. 2009;37(9):e67.
16. Brunak S, Engelbrecht J, Knudsen S. Prediction of human mRNA donor and acceptor sites from the DNA sequence. *J Mol Biol*. 1991;220(1):49-65.
17. Reese MG, Eeckman FH, Kulp D, Haussler D. Improved splice site detection in Genie. *J Comput Biol*. 1997;4(3):311-323.
18. Fairbrother WG, Yeh R-F, Sharp PA, Burge CB. Predictive identification of exonic splicing enhancers in human genes. *Science*. 2002;297(5583):1007-1013.
19. Dogan RI, Getoor L, Wilbur WJ, Mount SM. SplicePort--an interactive splice-site analysis tool. *Nucleic Acids Res*. 2007;35(Web Server issue):W285-291.